UNIVERSITY OF AMSTERDAM

UvA-DARE (Digital Academic Repository)

Shape oscillations in non-degenerate Bose gases - transition from the collisionless to the hydrodynamic regime.

Buggle, C.A.A.; Pedri, P.; von Klitzing, W.; Walraven, J.T.M.

Publication date
2005

Published in
Physical Review A

Link to publication

Citation for published version (APA):
Buggle, C. A. A., Pedri, P., von Klitzing, W., & Walraven, J. T. M. (2005). Shape oscillations in non-degenerate Bose gases - transition from the collisionless to the hydrodynamic regime. *Physical Review A*, *72*, 043610-1-10.

General rights
It is not permitted to download or to forward/distribute the text or part of it without the consent of the author(s) and/or copyright holder(s), other than for strictly personal, individual use, unless the work is under an open content license (like Creative Commons).

Disclaimer/Complaints regulations
If you believe that digital publication of certain material infringes any of your rights or (privacy) interests, please let the Library know, stating your reasons. In case of a legitimate complaint, the Library will make the material inaccessible and/or remove it from the website. Please Ask the Library: https://uba.uva.nl/en/contact, or a letter to: Library of the University of Amsterdam, Secretariat, P.O. Box 19185, 1000 GD Amsterdam, The Netherlands. You will be contacted as soon as possible.

UvA-DARE is a service provided by the library of the University of Amsterdam (https://dare.uva.nl)

Download date:10 Oct 2026

Shape oscillations in nondegenerate Bose gases: Transition from the collisionless to the hydrodynamic regime

Ch. Buggle,[1] P. Pedri,[2] W. von Klitzing,[1,*] and J. T. M. Walraven[1]
[1]*FOM Institute for Atomic and Molecular Physics, Kruislaan 407, 1098 SJ Amsterdam, The Netherlands and Van der Waals-Zeeman Institute of the University of Amsterdam, Valckenierstraat 65/67, 1018 XE The Netherlands*
[2]*Institut für Theoretische Physik III Universität Stuttgart, Pfaffenwaldring 57 V, 70550 Stuttgart, Germany*
(Received 17 May 2005; published 21 October 2005)

We investigate collective oscillations of nondegenerate clouds of ^{87}Rb atoms as a function of density in an elongated magnetic trap. For the low-lying $M=0$ monopole-quadrupole shape oscillation we measure the oscillation frequencies and damping rates. At the highest densities the mean free path is smaller than the axial dimension of the sample, which corresponds to collisionally hydrodynamic conditions. This allows us to cover the crossover from the collisionless to the hydrodynamic regime. The experimental results show good agreement with theory. We also analyze the influence of trap anharmonicities on the oscillations in relation to observed temperature dependencies of the dipole and quadrupole oscillation frequencies. We present convenient expressions to quantify these effects.

DOI: 10.1103/PhysRevA.72.043610 PACS number(s): 03.75.Kk, 05.30.Jp, 32.80.Pj

I. INTRODUCTION

Collisional hydrodynamics has gradually become an important issue for the understanding of experiments with dilute quantum gases. When the atomic mean free path is smaller than the characteristic dimensions of typical elongated atomic clouds, the gas properties depend on the local density field and exhibit collisional hydrodynamics rather than the collisionless dynamics of a nearly ideal gas [1,2]. For Bose gases and Bose-Fermi mixtures it is difficult to penetrate deeply into this collisional hydrodynamic regime as three-body molecule formation will give rise to the fast decay of the samples [1]. Therefore, the transition region between collisionless and hydrodynamic conditions is also of substantial practical importance.

The hydrodynamic flow of classical fluids was described as early as 1755 by the equation of motion of Euler [3]. The opposite limit of collisionless flow is equally well understood since the work of Maxwell and Boltzmann and the investigation of rarefied gas dynamics around the turn of the last century [2]. The transition regime between collisionless and hydrodynamic conditions deserves special attention as the crossover behavior is often nonintuitive as was already noted by Knudsen in 1908 [4]. With the availability of trapped ultracold gases there is a renewed interest in the collisional hydrodynamics. For nondegenerate quantum gases in harmonic traps the absence of the familiar wall-boundary condition of zero hydrodynamic flow at the sample edges gives rise to a very close phenomenological similarity with the superfluid hydrodynamics of Bose-Einstein condensates [1,5–7]. Collisional hydrodynamics also has to be considered in two-component Fermi gases near intercomponent Feshbach resonances, where the intercomponent scattering length is tuned to large values in order to optimize thermalization [8–11].

The onset of collisional hydrodynamics in a quantum gas, to the best of our knowledge, was first observed at MIT in measurements of the damping and frequency shifts of the low-lying $M=0$ quadrupole shape oscillation of cigar-shaped samples of the ^{23}Na quantum gas, just above the Bose-Einstein transition temperature T_c [12]. Similar results were obtained at the ENS-Paris with clouds of metastable triplet helium (He^*) [13]. A demonstration of the collisional crossover was given at JILA by measuring, for varying density, the damping of the center of mass oscillations of two distinguishable clouds of ^{40}K, passing in antiphase [14,15]. At AMOLF we showed how hydrodynamic conditions affect the BEC-formation process in elongated samples and can give rise to substantial shape oscillations of the condensates being formed [16,17]. Further, hydrodynamic conditions were shown to give rise to an anisotropic expansion of thermal Bose gases after switching off the confining field, which has important consequences for time-of-flight thermometry [18,19]. Hydrodynamic effects were observed more pronouncedly in the expansions of two-component Fermi gases tuned near an intercomponent Feshbach resonance [8–10]. Also the investigation of the macroscopic dynamics of two-component Fermi gases in the BCS-BEC transition region requires detailed understanding of the hydrodynamics [20–23].

In this paper we study the crossover from collisionless to hydrodynamic conditions in nondegenerate clouds of ^{87}Rb by measuring both the frequency shift and the damping of the low-lying $M=0$ quadrupole shape oscillation as a function of density. In accordance with theory [5–7], the frequency shifts down from $2\omega_z$ in the collisionless regime to $1.55\omega_z$ for collisionally hydrodynamic clouds, with ω_z the axial frequency of our trap. Most of the shift occurs over a narrow range of densities around the crossover density, where the mean free path becomes comparable to the axial size of the sample. At this density also the strongest damping is observed. All our data were taken for temperatures $T>2T_c$ to avoid precursor phenomena close to the BEC tran-

*Present address: IESL-FORTH, Vassilika Vouton, 711 10 Heraklion, Greece.

 ©2005 The American Physical Society

sition [24]. Hence, although the collisions are quantum (i.e. *s* wave), the gas is statistically classical. As we observed a temperature dependence of the oscillation frequencies, we derive theoretical expressions to include the influence of trap anharmonicities, which cause this effect. These expressions allow a numerical evaluation for regular potentials. Further, they allow us to derive convenient analytic approximations that apply to *any* elongated Ioffe-Pritchard trap.

II. BACKGROUND

For quantum gases well above the degeneracy temperature, all oscillatory modes are solutions to the classical Boltzmann equation [1,25]

$$\frac{\partial f}{\partial t} + \mathbf{v}\cdot\boldsymbol{\nabla}_{\mathbf{r}} f + \frac{\mathbf{F}}{m}\cdot\boldsymbol{\nabla}_{\mathbf{v}} f = I_{\mathrm{coll}}[f], \tag{1}$$

where $f=f(t,\mathbf{r},\mathbf{v})$ is the phase-space distribution function with $\mathbf{r}=\{r_j\}=(x,y,z)$ and $\mathbf{v}=\{v_j\}$ the position and momentum vectors, m is the atomic mass, and $\mathbf{F}(\mathbf{r})=-\nabla_{\mathbf{r}}U(\mathbf{r})$ the force of the trapping potential $U(\mathbf{r})$; $I_{\mathrm{coll}}[f]$ is the classical collisional integral. For the case of *s*-wave collisions with an energy-independent elastic-scattering cross section σ the collision integral takes the form

$$I_{\mathrm{coll}}[f] = \frac{\sigma}{4\pi}\int d\mathbf{v}_1\, d\Omega' |\mathbf{v}_1 - \mathbf{v}|[f_1' f' - f_1 f] \tag{2}$$

and describes, for a given position and time, the effect of elastic collisions between a pair of atoms with initial velocities $\mathbf{v}$ and $\mathbf{v}_1$ and final velocities $\mathbf{v}'$ and $\mathbf{v}_1'$. The solid angle Ω' gives the direction of the final relative velocity with respect to the initial one.

For *isotropic* harmonic traps the normal modes are multipoles of order $(L;M)$ [6]. Oscillations in the dipole mode $(L=1)$ are commonly used for measuring trap frequencies by observing the motion of the center of mass of trapped clouds as a function of time. In harmonic traps these oscillations are undamped, since for any pair of atoms also their center of mass oscillates at the trap frequency ω. As noted in Refs. [6,7], Boltzmann obtained in 1897 the surprising result that for isotropic harmonic traps also the monopole (or "breathing") mode $(L=0)$ is undamped, oscillating at frequency 2ω, *independent* of the density. The next normal mode solutions are shape oscillations $(L\geqslant 2)$. In the hydrodynamic limit they are (like the dipole mode) both irrotational and divergence free [6,7], and therefore also undamped. They oscillate at frequency $\sqrt{L}\omega$ [26]. In the collisionless regime they are again undamped but oscillate at frequency $L\omega$. This difference in frequency results in damping in the transition regime [27] due to the collisional relaxation towards equilibrium.

For *elongated* harmonic traps, with axial direction z and radial coordinate $\rho=(x^2+y^2)^{1/2}$, we distinguish three $(L=1;\ M=0,\pm 1)$ dipole modes, oscillating uncoupled and undamped at frequencies ω_z and ω_ρ. In the hydrodynamic limit, the monopole mode is coupled to the $(L=2;\ M=0)$ quadrupole mode. Decoupling in terms of irrotational solutions yields [5–7]

$$\omega^2 = \tfrac{1}{3}[5\omega_\rho^2 + 4\omega_z^2 \pm \sqrt{25\omega_\rho^4 + 16\omega_z^4 - 32\omega_\rho^2\omega_z^2}]. \tag{3}$$

In the experiment described in this paper, we study the low-lying $M=0$ coupled monopole-quadrupole mode, corresponding to the minus sign in Eq. (3). In this mode the radial size oscillates in antiphase with the axial size. For shortness we will refer to it as the "quadrupole" mode with frequency ω_Q in all regimes, although in the collisionless limit the axial and radial motion decouple and the overall behavior is to be considered as a superposition of "one-dimensional (1D) breathing modes", showing dephasing behavior. This dephasing can be avoided by exciting a pure axial oscillation. As follows directly from Eq. (3), in the limit of very elongated clouds $(\omega_\rho \gg \omega_z)$ we have $\omega_Q=\sqrt{12/5}\omega_z \approx 1.55\omega_z$.

The transition regime is less obvious. Describing the oscillation phenomenologically by $e^{-i\omega t}$ the crossover takes the form [27]

$$\omega^2 = \omega_{\mathrm{cl}}^2 + \frac{\omega_{\mathrm{hd}}^2 - \omega_{\mathrm{cl}}^2}{1 - i\omega\tilde{\tau}}, \tag{4}$$

where $\omega=\omega'+i\omega''$ is the complex quadrupole frequency for a given thermal relaxation time $\tilde{\tau}$; ω_{hd} and ω_{cl} are the (real) frequencies of this mode in the hydrodynamic $(\omega'\tilde{\tau}\ll 1)$ and collisionless $(\omega'\tilde{\tau}\gg 1)$ limits, respectively.

To have an intuitive picture of the solutions of Eq. (4) one can separate the real and imaginary parts of ω and make the identification $(\omega_Q=\omega',\ \Gamma=-\omega'')$. For $\Gamma/\omega_Q \ll 1$ we can approximate the imaginary part of the solution by the convenient form

$$\Gamma \simeq \frac{\tilde{\tau}}{2}\frac{\omega_{\mathrm{hd}}^2 - \omega_{\mathrm{cl}}^2}{1 + \omega_{\mathrm{cl}}^2\tilde{\tau}^2}, \tag{5}$$

which underestimates the maximum damping by 23%. The solution for the real part of Eq. (4) can be heuristically, but fairly accurately $(\pm 0.3\,\%)$ described by

$$\omega_Q \simeq \omega_{\mathrm{hd}} + (\omega_{\mathrm{cl}} - \omega_{\mathrm{hd}})(2/\pi)\arctan(\omega_{\mathrm{cl}}^2\tilde{\tau}^2). \tag{6}$$

We define the "crossover point" as the point where maximum damping occurs and the frequency is at the intermediate value $\omega_Q=\frac{1}{2}(\omega_{\mathrm{cl}}+\omega_{\mathrm{hd}})$. From Eqs. (5) and (6) this is seen to occur at the relaxation time $\tilde{\tau}=\tilde{\tau}_0$, where $2\omega_z\tilde{\tau}_0=1$.

Equation (4) can be obtained from the Boltzmann equation in the relaxation time approximation [28,29], where the collisional integral is replaced by

$$I_{\mathrm{coll}}[f] \simeq -(f - f_{\mathrm{le}})/\tau. \tag{7}$$

Here τ is the relaxation time and $f_{\mathrm{le}}=f_{\mathrm{le}}(t,x,v)$ the local thermal distribution, which has an isotropic momentum distribution [30]. For harmonic traps one has [28]

$$\tau^{-1} = \frac{\sqrt{2}}{5}\tau_c^{-1}, \quad \text{where } \tau_c^{-1} = \sqrt{2}n_0\bar{v}_{\mathrm{th}}\sigma \tag{8}$$

is the elastic collision rate at the trap center [25], with $\bar{v}_{\mathrm{th}}=(8k_BT/\pi m)^{1/2}$ the mean thermal velocity at temperature T, n_0 the central density.

To arrive at Eq. (4) the relaxation time has to be renormalized by a factor that depends both on the cloud shape and

the mode considered. For the $M=0$ quadrupole mode in very elongated harmonic traps one finds $\tilde{\tau}=6/5\tau$ [28,29].

III. EXPERIMENT

In our experiment we typically load 10^{10} atoms from the ^{87}Rb source described in Ref. [31] into a magneto-optical trap. After an optical molasses stage we optically pump the atoms into the fully stretched ($5S_{1/2}$, $F=2$, $m_F=2$) hyperfine state and transfer the cloud into a Ioffe-Pritchard trap with frequencies $\omega_z/2\pi=7$ Hz and $\omega_\rho/2\pi=8$ Hz and central field $B_0=37$ G. Any remaining population in the $m_F=1$ magnetic sublevel is removed by the gravitational sag. Then, we radially compress the cloud, changing the trap parameters to $\omega_\rho/2\pi=19$ Hz at $B_0=8$ G. After a thermalization time of 100 ms we add, in a linear ramp over 0.5 ms, a magnetic field $B_m=487$ mG, rotating at a frequency of $\nu_m=7$ kHz orthogonally to the trap axis, using the approach described in Ref. [32]. This gives rise to a time-averaged-potential (TAP) field with offset $B_{0,m}\equiv(B_m^2+B_0^2)^{1/2}$ and frequencies

$$\omega_{\rho,m}=\omega_\rho\frac{(1+0.5b^2)^{1/2}}{(1+b^2)^{3/4}}, \tag{9}$$

$$\omega_{z,m}=\omega_z\frac{1}{(1+b^2)^{1/4}}, \tag{10}$$

where $b=B_m/B_0$ is the modulation depth [32].

We continue the compression to $\omega_{z,m}/2\pi=16.8$ Hz, $\omega_{\rho,m}/2\pi=474$ Hz and $B_{0,m}=634$ mG ($B_0=406$ mG, $b=1.2$). Then, we cool the sample by forced rf evaporation to the final temperature of a few microkelvin. After reducing the density to the desired level by laser depletion [33], the sample is thermalized during plain evaporation periods of up to 2.5 s, which is sufficiently long even for our lowest densities. We then raise the rf-shield energy by a factor of 7 to avoid evaporation losses during the measurements.

It is important to note here that the harmonic range $\rho_{0,m}$ where Eqs. (9) and (10) hold, is proportional to the amplitude of the rotating field: $\rho_{0,m}=B_m/\alpha$, where α is the radial gradient of the Ioffe quadrupole field. For regions outside the harmonic range the frequencies revert to the unmodulated ones [34]. This implies a *minimum* required value for B_m to assure that the harmonic radius of the TAP field exceeds the thermal size of the sample.

A. Excitation of the quadrupole mode

To excite the quadrupole mode we remove the modulation field B_m and observe the oscillation in a static potential. The advantage of the TAP approach is the rapid switching between trap frequencies, which is possible because both B_m and B_0 are generated by trim coils. The main currents of the Ioffe-Pritchard trap remain untouched. Further, this approach offers definite knowledge of phase and amplitude. After transfer into the static potential the cloud starts to oscillate inwards as a cosine function with zero phase offset as can be seen in Fig. 1.

As we remove the modulation, we simultaneously increase the central field to $B_0=900$ mG in order to keep ω_ρ constant. The procedure is done with a linear ramp of duration $\tau_{sw}=230$ μs. This is slow enough to avoid switch-off depolarization and still much faster than the axial oscillation time $\omega_z\ll\tau_{sw}^{-1}\ll\omega_{Larmor}$. Thus, after switching ω_z, the gas finds itself diabatically in an axially tighter potential. The axial trap frequency has increased to $\omega_z/2\pi=21.1$ Hz, which changes the aspect ratio to $\omega_\rho/\omega_z\approx 23$ and puts us well into the elongated trap limit of Eq. (3).

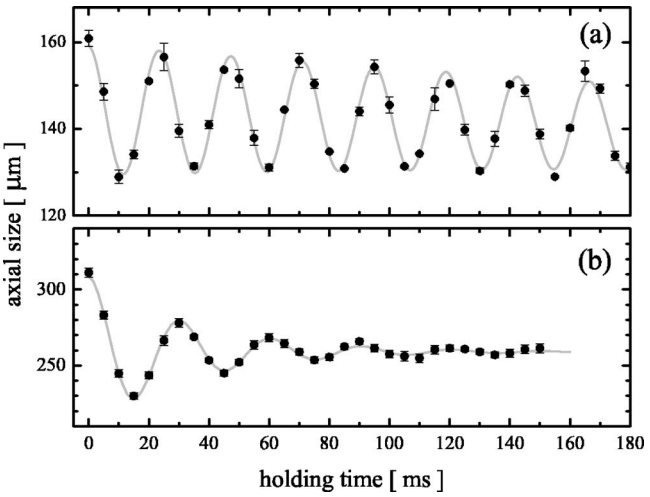

FIG. 1. Typical quadrupole oscillation traces for fitting frequency and damping; raw data acquired at a temperature of 2 μK: (a) Low density data ($n_0=1.7\times10^{11}$ cm^{-3}) with a fit function (gray line) resulting in $\omega_Q/\omega_z=2.0$ and $\Gamma/\omega_z=0.01$. Each point represents the average of three absorption images. (b) High density data ($n_0=1.1\times10^{14}$ cm^{-3}) with a fit function (gray line) resulting in $\omega_Q/\omega_z=1.6$ and $\Gamma/\omega_z=0.22$. Each point represents the average of 15 phase contrast images. The error bars represent the error in the mean.

In this way we excite a pure axial oscillation, at least in the collisionless limit. In the hydrodynamic limit, in principle, both the low-lying and the high-lying monopole-quadrupole modes could be excited. However, since even at our highest densities, *radially* we remain in the collisionless regime, the high-lying mode cannot be excited due to the lack of coupling.

If the extent of the cloud prepared in the TAP-modulated magnetic field reaches significantly beyond $\rho_{0,m}$, its density profile deviates from a Gaussian. Transferring that distribution in the described way into the static magnetic field leads to excitation of higher modes. If additionally the thermal size of the cloud also exceeds the harmonic range of the static potential (which is *not* related to $\rho_{0,m}$), both anharmonicities will add to the excitation of higher modes. However, these modes oscillate at much higher frequencies and damp accordingly faster than the quadrupole mode under investigation.

For our highest-density samples, together with the condition $T\gtrsim 2T_c$, we have $\rho_{0,m}\gtrsim 10$ μm, which implies a required TAP amplitude $B_m>350$ mG. The value of $B_m=487$ mG, used in the experiment, represents our technical limit, and corresponds to the harmonic $1/e$ size of a thermal cloud at a temperature of 9 μK. To assure that fitted values for frequency and damping are unaffected by higher

modes, we neglect the first two cycles of oscillation traces acquired at temperatures above 7 μK, and the first cycle for traces acquired above 4 μK. For lower temperatures also the first cycle is analyzed. Note that the precise reproducibility of the starting phase of our oscillations allows this procedure without degrading the quality of the fits.

B. Description of the trapping field

During the observation of the quadrupole oscillation the cloud resides in a potential given by $U(\mathbf{r})=\mu_B[B(\mathbf{r})-B_0]+mgy$ for the chosen Zeeman level in this experiment. Here μ_B is the Bohr magneton and g the gravity acceleration along the vertical direction (y direction). For elongated Ioffe-Pritchard traps the modulus of the trapping field $B(\mathbf{r})$ is accurately described by [35,36]

$$B(x,y,z)=\sqrt{(B_0+\beta z^2)^2+\alpha^2(x^2+y^2)+4\alpha\beta xyz}, \quad (11)$$

where $B_0=0.9$ G and $\alpha=353$ G/cm are defined above and $2\beta=274$ G/cm^2 is the axial curvature. To our knowledge α and β were constant throughout the measurements to within 0.1%; B_0 was monitored to be constant to within 1%. Expanding Eq. (11) around the trap center and keeping the leading nonlinearities [36], the potential can be written as

$$U(\rho,z)=\tfrac{1}{2}m\left[\omega_z^2z^2\left(1-\tfrac{1}{2}\rho^2/\rho_0^2\right)+\omega_\rho^2\rho^2\left(1-\tfrac{1}{4}\rho^2/\rho_0^2\right)\right]+\cdots, \quad (12)$$

where $m\omega_z^2=2\mu_B\beta$, $m\omega_\rho^2=\mu_B\alpha^2/B_0$ and $\rho_0=B_0/\alpha=25$ μm the harmonic radius [37].

C. Detection procedure

Two imaging methods are used to observe the oscillations. For our highest-density samples we use phase-contrast imaging with red-detuned light. For densities $n_0>5\times10^{13}$ cm^{-3} a proper contrast is obtained at a detuning of -3 GHz, where the detection is essentially nondestructive [38]. This allows us to register the oscillations in a sequence of 31 images at 5 ms intervals, taking advantage of the fast "kinetics" imaging mode of our camera [39]. For lower densities the phase contrast method cannot be used because, at the (smaller) detunings required to maintain adequate phase contrast, photoassociation losses disturb the measurements [40].

For densities $n_0<5\times10^{13}$ cm^{-3}, we used repetitive absorption imaging on the $(5S_{1/2},F=2)\leftrightarrow(5P_{3/2},F=3)$ transition (D_2-line) [42], varying the holding time of the cloud after excitation of the oscillation. The images were taken *in situ*, just before releasing the cloud from the trap [43]. We apply the usual method of background subtraction and level normalization to process the images [45,46]. To retrieve the column density profile $n_2(y,z)$ and the axial and radial Gaussian $1/e$ sizes L_e and R_e, we fit a two-dimensional Gaussian expression to the optical thickness distribution of our images. The central density follows with $n_0=n_2(0,0)/\sqrt{\pi R_e^2}$ and, with Eq. (8), the relaxation time can be expressed as

$$\omega_z\tilde{\tau}=\frac{3}{2}\frac{\omega_z}{\omega_\rho}\frac{\pi\ \nu}{n_2(0,0)\sigma}. \quad (13)$$

Note that this expression does not depend explicitly on the gas temperature. The collision cross section is $\sigma=8\pi a^2$ in the zero temperature limit and is calculated with the value $a=98.98(4)a_0$ for the s-wave scattering length [47].

To acquire sufficient statistics, at least 30 images are taken to retrieve one oscillation trace for a given density and each trace is acquired at least three times. Because the crossover happens over a narrow range of densities, great care was taken to reproduce the initial conditions from shot to shot. This is done by adjusting the density using laser depletion in a feedback loop with the experimental result of the previous shot [33]. Although this procedure increases the shot to shot fluctuations, long-term drift is virtually eliminated. With this procedure the atom number could be long-term stabilized within a standard deviation of better than 1%. By fitting the expression for an exponentially damped cosine function to the trace (see Fig. 1), we retrieve the experimental values for the frequency ω_Q and damping rate Γ of the quadrupole mode for the selected density.

D. Accuracy of density and temperature determination

The *absolute* accuracy of $n_2(0,0)$ is estimated to be $\sim$30% [48]. The phase contrast images are calibrated against absorption images of expanded clouds taken 15 ms after release from the trap at zero detuning. This procedure presumes the conservation of atom number during the expansion.

In our analysis we account to leading order for the corrections associated with trap anharmonicities. For temperatures much lower than the harmonic temperature $T_0=\mu_BB_0/k_B=60$ μK, Eq. (12) becomes sufficiently accurate to describe the cloud shape. In this limit the column density on the trap axis (to leading order in the x integration) can be expressed for $z^2\ll 2k_BT/m\omega_z^2$ as

$$n_2(0,z)\simeq n_2(0,0)\exp\left(-\frac{m\omega_z^2z^2}{2k_BT}\left(1-\tfrac{1}{2}T/T_0\right)\right), \quad (14)$$

where $T/T_0=\langle x^2\rangle/\rho_0^2=k_BT/\mu_BB_0$ with $\langle x^2\rangle=k_BT/m\omega_\rho^2$ the variance of the thermal distribution of the cloud along the x axis in the harmonic limit.

From Eq. (14) we estimate the $1/e$-axial-size L_e that will be obtained by fitting a Gaussian to the axial column density profile of the cloud, $L_e=L/\left(1-\frac{1}{4}T/T_0\right)$ with L defined by $L^2=2k_BT/m\omega_z^2$ [49]. The temperature follows with the expression

$$-k_BT\simeq\tfrac{1}{2}m\omega_z^2L_e^2\left(1-\tfrac{1}{2}T/T_0\right). \quad (15)$$

Hence, for a temperature of 6 μK the harmonic approximation overestimates the temperature by $\sim$5%. The correction in the central column density is smaller. Numerically we established that the fit of a 2D Gaussian underestimates the central column density by $\sim$1.4% at $T/T_0=0.1$. As these corrections are small, there is no need to go beyond the leading order of anharmonic correction to retrieve these quanti-

ties. For measuring oscillation frequencies the situation is different because these can be measured to high precision.

Mean-field broadening of the distribution is small [50]. Calculating the variance $\langle z^2\rangle=\frac{1}{2}L^2$ using the recursive expression for the density to first order in mean field $U_{\rm mf}(\mathbf{r})=2v_0n(\mathbf{r})$, leads for $T\ll T_0$ to

$$\tfrac{1}{2}m\omega_z^2L^2 \simeq k_BT + E_{\rm mf}, \tag{16}$$

where $E_{\rm mf}=v_0\int n^2(\mathbf{r})d\mathbf{r}/\int n(\mathbf{r})d\mathbf{r}=v_0n_0/\sqrt{8}$ is the trap averaged interaction energy with $v_0=(4\pi\hbar^2/m)a$ the interaction coupling constant [1]. Equivalently, treating the mean field as an effective potential we may write

$$k_BT=\tfrac{1}{2}m\omega_z^2L^2(1-\xi), \tag{17}$$

where $\xi=E_{\rm mf}/(k_BT+E_{\rm mf})$ is the mean field correction constant. For the data point with the highest mean field ($n_0=1.1\times10^{14}$ cm^{-3}, $T=2$ μK) we calculate $\xi=0.007$. Therefore, mean-field corrections are at least one order of magnitude smaller that the anharmonic corrections and are discarded in this paper.

IV. ANHARMONIC FREQUENCY SHIFTS

As we operate at temperatures well above T_c, we pay special attention to the issue of trap anharmonicities. We follow the path of argumentation as presented in [28,30] to derive expressions for the anharmonic shifts. These are both temperature and mode dependent and can also depend on the density. The expressions are suitable for numerical evaluation provided the first and second spatial derivatives of the trapping potential are known.

To describe the dynamical evolution of an observable $\chi=\chi(\mathbf{r},\mathbf{v})$ it is multiplied by Eq. (1) and averaged over the phase space

$$\frac{d}{dt}\langle\chi\rangle-\langle\mathbf{v}\cdot\boldsymbol{\nabla}_r\chi\rangle-\frac{1}{m}\langle\mathbf{F}\cdot\boldsymbol{\nabla}_v\chi\rangle=-\frac{\langle\chi\rangle-\langle\chi\rangle_{\rm le}}{\tau}, \tag{18}$$

where

$$\langle\chi\rangle(t)=\frac{1}{N}\int\chi(\mathbf{r},\mathbf{v})f(t,\mathbf{r},\mathbf{v})d^3r\,d^3v, \tag{19}$$

with N the number of atoms. By choosing the correct set of observables, it is possible to obtain a closed set of equations that describes the dynamics of these observables.

A. Dipole mode ($L=1$)

To investigate the effect of trap anharmonicities on the dipole mode oscillation, we make the Ansatz

$$f(t,\mathbf{r},\mathbf{v})=f_0(r_i-a_i,v_i-\dot{a}_i), \tag{20}$$

where $f_0(\mathbf{r},\mathbf{v})=\mathcal{C}\exp(-[mv^2/2+U(\mathbf{r})]/k_BT)$ is the equilibrium distribution function with $\mathcal{C}$ the normalization factor and $a_i=a_i(t)$. We choose $\chi=v_i$ and obtain the following set of equations:

$$\frac{d}{dt}\langle v_i\rangle-\frac{1}{m}\langle F_i(\mathbf{r})\rangle=0, \tag{21}$$

where

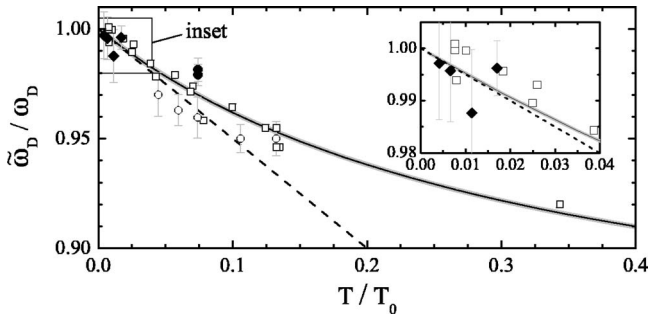

FIG. 2. Scaled frequencies $\tilde{\omega}_D/\omega_D$ for the axial dipole mode versus temperature. The gray line corresponds to the evaluation of Eq. (24). The leading slope (dashed line) is given by Eq. (25). Open circles: phase contrast measurements; closed circles: absorption imaging measurements, both acquired with thermal clouds. Diamonds: measurements with Bose-Einstein condensates, using absorption imaging. Open squares: results acquired at ENS-Paris [51].

$$\langle v_i\rangle=\dot{a}_i \text{ and } \langle F(\mathbf{r})\rangle=\langle F(\mathbf{r}+\mathbf{a})\rangle_0. \tag{22}$$

Analogously to Eq. (19) we denote with $\langle\chi\rangle_0$ the average on the phase space using the equilibrium distribution $f_0(\mathbf{r},\mathbf{v})$. Expanding up to first order around the equilibrium position $a_i=0$, we obtain

$$\ddot{a}_i+\frac{1}{m}\sum_j\langle U''_{ij}\rangle_0a_j=0, \tag{23}$$

where $U''_{ij}=\partial^2U/\partial r_i\partial r_j$. Restricting ourselves to potentials with $\langle U''_{ij}\rangle_0=0$ for $i\neq j$, we obtain for the effective frequencies of the dipole modes

$$\tilde{\omega}_{iD}^2=\frac{1}{m}\langle U''_{ii}\rangle_0. \tag{24}$$

Substituting Eq. (12) for the potential into Eq. (24) we obtain for the leading anharmonic shift in the z direction

$$\tilde{\omega}_{zD}\simeq\omega_z\left(1-\tfrac{1}{2}T/T_0\right). \tag{25}$$

This expression is shown as a dashed line in Fig. 2. The integral in Eq. (24) is readily evaluated numerically using Eq. (11) and requires as input parameters only the values for α, β, and B_0. The resulting curve is shown as the solid line in Fig. 2. The curve follows the trend of our measurements of center-of-mass oscillations as well as data obtained in Paris [51].

The zero temperature limit of $\tilde{\omega}_{zD}$ is largely fixed by measurements with Bose-Einstein condensates, which reproduced within 1% over a period of one year. Its value is used to calibrate ω_z and the related β coefficient. We have no explanation for the remaining deviations for the points taken with thermal samples at higher temperatures [52]. We cannot trace them back to insufficient mechanical or electronic stability of our trap. Nonexponential contributions to the damping may account for a systematic error in the frequency, but should be less than 1%. We speculate that possibly the temperature determinations of the phase contrast measurements could be affected by a molecular contribution to the phase contrast, which tends to narrow down the distribution and

results in an underestimated value for the temperature. This results from the distribution of pairs, that can photoassociate, which is proportional to the square of the atomic density.

B. Surface modes ($L=0$, $L=2$)

In order to calculate the anharmonic shifts for the breathing and the two quadrupole modes we make the Ansatz

$$f(t,\mathbf{r},\mathbf{v}) = \frac{1}{\prod_j b_j\sqrt{\theta_j}} f_0\left(\frac{r_i}{b_i}, \frac{[v_i - (\dot{b}_i/b_i)r_i]}{\theta_i^{1/2}}\right), \tag{26}$$

where b_i and θ_i are time-dependent variables. The parameters b_i take into account shape deformation of the density cloud whereas the parameters θ_i allow an anisotropic momentum distribution which is crucial to calculate the correct frequencies. We choose $\chi=v_i r_i$ and obtain the following set of equations:

$$\ddot{b}_i\langle r_i^2\rangle_0 - \frac{\theta_i}{b_i}\langle v_i^2\rangle_0 - \frac{1}{m}\langle F_i(b_j r_j) r_i\rangle_0 = 0. \tag{27}$$

We impose the stationary solution and find the relation

$$\langle v_i^2\rangle_0 = -\frac{1}{m}\langle F_i(r_j) r_i\rangle_0. \tag{28}$$

Then choosing $\chi=[v_i-(\dot{b}_i/b_i)r_i]^2$ yields

$$\dot{\theta}_i + 2\frac{\dot{b}_i}{b_i}\theta_i = -\frac{\theta_i - \bar{\theta}}{\tau}, \tag{29}$$

where $\bar{\theta}=(\Sigma_i\theta_i)/3$.

Let us now focus our attention on two extreme regimes.

1. Collisionless limit

In the collisionless limit ($\tau\to\infty$) we obtain the relation

$$\theta_i = \frac{1}{b_i^2}, \tag{30}$$

and finally,

$$\ddot{b}_i + \frac{1}{b_i^3}\frac{\langle F_i(r_j) r_i\rangle_0}{m\langle r_i^2\rangle_0} - \frac{\langle F_i(b_j r_j) r_i\rangle_0}{m\langle r_i^2\rangle_0} = 0. \tag{31}$$

Linearizing these equations and looking for solution of the form $e^{-i\omega t}$ we obtain the three frequencies. In order to do this explicitly we define the quantities

$$A_{ii} = \frac{3}{m}\frac{\langle r_i U_i'\rangle_0}{\langle r_i^2\rangle_0}, \tag{32}$$

where $U_i' = \partial U/\partial r_i$, $A_{ij}=0$ for $i\neq j$ and

$$B_{ij} = \frac{1}{m}\frac{\langle r_i r_j U_{ij}''\rangle_0}{\langle r_i^2\rangle_0}, \tag{33}$$

where $U_{ij}'' = \partial^2 U/\partial r_i \partial r_j$; note that, in general, $B_{ij}\neq B_{ji}$. We have to solve

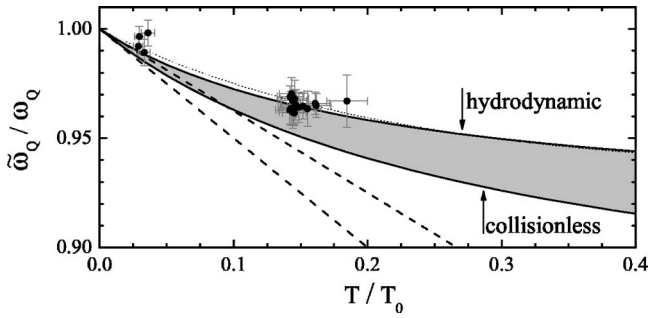

FIG. 3. Scaled frequencies $\tilde{\omega}_Q/\omega_Q$ for the quadrupole mode versus temperature. The gray sector corresponds to Eq. (37) evaluated for the crossover regime (see Sec. IV B 3) with the collisionless and hydrodynamic limits indicated. The dashed lines show the leading slopes given by Eqs. (40) and (44). All data points correspond to collisionless conditions. The dotted line is used to scale all quadrupole frequency data to zero temperature.

$$|A + B - \tilde{\omega}^2 I| = 0, \tag{34}$$

where I is the identity matrix, in order to obtain the frequencies. For the quadrupole modes with $M=\pm 2$ we find

$$\tilde{\omega}_{Q2}{}^2 = A_{xx} - A_{xy} + B_{xx} - B_{xy}, \tag{35}$$

whereas for the modes with $M=0$ we have

$$\tilde{\omega}_B{}^2 = \mu + \sqrt{\mu^2 - \Delta} \tag{36}$$

$$\tilde{\omega}_Q{}^2 = \mu - \sqrt{\mu^2 - \Delta}, \tag{37}$$

where

$$\mu = (A_{xx} + A_{xy} + A_{zz} + B_{xx} + B_{xy} + B_{zz})/2, \tag{38}$$

$$\Delta = (A_{xx} + A_{xy} + B_{xx} + B_{xy})(A_{zz} + B_{zz}) - 2(A_{xz} + B_{xz})(A_{zx} + B_{zx}). \tag{39}$$

Here we used $\langle U_{ij}''\rangle_0=0$ for $i\neq j$. An analytic approximation for the leading anharmonic shift of the $M=0$ quadrupole mode is obtained by substituting Eq. (12) for the trap potential,

$$\tilde{\omega}_Q \simeq \omega_Q\left(1 - \tfrac{1}{2}T/T_0\right), \tag{40}$$

where ω_Q is the frequency in the harmonic limit. Note that at this level of the approximation the relative shift coincides with that of the dipole mode. The result of the numerical averages based on Eq. (11) is shown as the lower solid line in Fig. 3. The lower dashed line corresponds to the leading shift given by Eq. (40).

Comparison with the experimental points in Fig. 3 shows agreement as far as the trend of the shift is concerned but a systematic deviation for the slope. This discrepancy can be eliminated by presuming that our axial trap frequency ω_z is underestimated by 1.5%. However, such a correction cannot be justified on the basis of the limited set of data for the dipole mode [52].

2. Hydrodynamic limit

In the hydrodynamic regime ($\tau \to 0$) the local equilibrium is always maintained, which implies that $\theta_i = \bar{\theta}$. In this case we obtain the relation

$$\theta_i = \bar{\theta} = \frac{1}{\prod_i b_i^{2/3}}, \tag{41}$$

and therefore

$$\ddot{b}_i + \frac{1}{b_i(\prod_j b_j)^{2/3}} \frac{\langle F_i(r_j) r_i \rangle_0}{m\langle r_i^2 \rangle_0} - \frac{\langle F_i(b_j r_j) r_i \rangle_0}{m\langle r_i^2 \rangle_0} = 0. \tag{42}$$

By linearizing around the equilibrium we find the frequencies for the $M = \pm 2$ modes and the two $M = 0$ monopole-quadrupole modes. In this case we have to define the A_{ij} matrix as

$$A_{ii} = \frac{5}{3m} \frac{\langle r_i U_i' \rangle_0}{\langle r_i^2 \rangle_0} \text{ and } A_{ij} = \tfrac{2}{5} A_{ii}. \tag{43}$$

Note that A_{ij} does not depend on j. The matrix B_{ij} is the same as in the collisionless case. Solving the determinant Eq. (34) leads again to Eqs. (35)–(37) for the frequencies and Eqs. (38) and (39) for μ and Δ. Only the expressions for the matrix elements A_{ij} have changed. Substituting Eq. (12) for the trap potential we find for the leading anharmonic shift of the hydrodynamic $M = 0$ quadrupole mode

$$\tilde{\omega}_Q \simeq \omega_Q \left(1 - \tfrac{3}{8} T/T_0\right), \tag{44}$$

which has a slightly weaker slope than in the collisionless case. The result of the numerical averages based on Eq. (11) are shown as the upper solid line in Fig. 3. The upper dashed line corresponds to the leading shift given by Eq. (44).

A comparison with experiment requires densities $n_0 > 4 \times 10^{14}$ cm^{-3} at a temperature $T = 4$ μK, to have $2\omega_z \tilde{\tau} < 0.1$, which is about three times our maximum density. At our highest density of $n_0 = 1.3 \times 10^{14}$ cm^{-3}, we calculate a three-body decay rate of $\dot{N}/N = 2\sqrt{3} L n_0^2 \approx 1$ s^{-1}, with $L = 1.8(5) \times 10^{-29}$ cm^6 s^{-1} the three-body rate constant in the Bose-condensed state [53]. At a three times higher density, the decay rate renders the acquisition of data at approximately constant density impossible for ^{87}Rb.

3. Crossover regime

In the crossover region, the same approach can be used, but after linearizing, one has to look for solutions of the form $e^{-i\omega t}$ with a complex ω. For the $M = 0$ modes this leads to the equation

$$\left(C[\omega] - \frac{i}{\tau} D[\omega]\right)\left(E[\omega] - \frac{i}{\tau} F[\omega]\right) = 0, \tag{45}$$

where $C[\omega] = \omega(\omega^2 - \omega_{\mathrm{cl:B}}^2)(\omega^2 - \omega_{\mathrm{cl:Q}}^2)$, $D[\omega] = (\omega^2 - \omega_{\mathrm{hd:B}}^2)(\omega^2 - \omega_{\mathrm{hd:Q}}^2)$, $E[\omega] = \omega(\omega^2 - \omega_{\mathrm{cl:Q2}}^2)$, and $F[\omega] = (\omega^2 - \omega_{\mathrm{hd:Q2}}^2)$. Each term represents two equations since they contain real and imaginary parts. For an elongated cigar-shape trap it is possible to write the frequencies in the form of Eq. (4) with rescaled relaxation time $\tilde{\tau} = (\omega_{\mathrm{cl:B}}^2 / \omega_{\mathrm{hd:B}}^2)\tau$, which reaches the value $\tilde{\tau} = 6/5\,\tau$ in the harmonic limit. The numerically calculated results of temperature induced shifts, based on Eq. (11) in the crossover regime, is represented by the gray sector in Fig. 3.

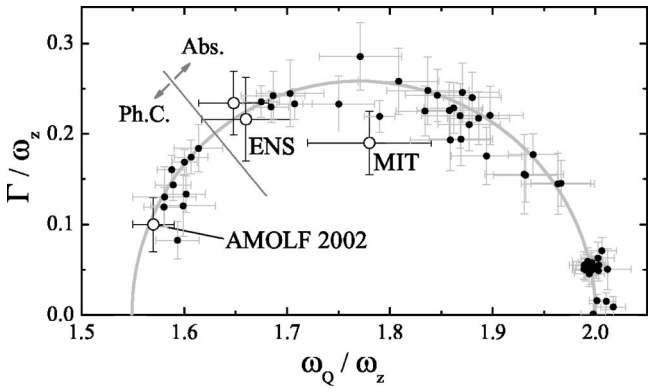

FIG. 4. Damping (raw data) versus frequency (extrapolated) for the quadrupole mode. Open circles: data acquired at MIT [45], ENS [13], and AMOLF [16]. The solid line is corresponds to the crossover expression Eq. (4). The data to the left of the straight line are obtained with phase contrast (Ph.C.) imaging, those on the right with absorption (Abs.) imaging. The error bars represent a 95% confidence interval of the fit.

A comparison with experiment is beyond the scope of this paper because, after scaling to ω_Q, the two limiting cases are spaced by only $\sim 1\%$. Therefore, not only $\tilde{\omega}_Q$ has to be determined to an accuracy much better than 1%, but also the scaling parameter ω_Q. In the limiting cases the latter is fully determined by the trap frequency (i.e. $\omega_{\mathrm{cl}} = 2\omega_z$ and $\omega_{\mathrm{hd}} \approx 1.55\omega_z$). However, in the crossover region knowledge of $\tilde{\tau}$ to much better than 1% is required to calculate ω_Q from Eq. (6) to adequate precision.

V. RESULTS AND DISCUSSION

We took all our data with the same trap parameters and the same excitation procedure, but at various temperatures. Starting the evaporation with a large atom number and using "tight" trapping parameters we could reach high densities and thus study the full crossover. However, this choice for a tight trap made us sensitive for anharmonic shifts as discussed in Sec. IV [54]. Therefore, we extrapolate all frequency data to the zero-temperature limit ($\tilde{\omega}_Q \to \omega_Q$) using the dotted curve in Fig. 3. This yields the best estimate for the value in the harmonic limit of our potential. The correction curve is based on the temperature dependence observed for our data in the collisionless regime ($2\omega_z \tilde{\tau} > 10$, see Fig. 5), where we may presume $\omega_Q = 2\omega_z$. In this way systematic deviations of our results from the curves in Figs. 4 and 5(b) were substantially reduced.

In Fig. 4 we plot the observed, scaled damping rates Γ/ω_z versus the extrapolated quadrupole frequencies normalized to the axial trap frequency, ω_Q/ω_z. The drawn curve corresponds to the crossover expression, Eq. (4) with $\omega_{\mathrm{cl}} = 2\omega_z$ and $\omega_{\mathrm{hd}} = 1.55\omega_z$. Plots of the same experimental data and the exact solutions of Eq. (4) separately against $2\omega_z\tilde{\tau}$ are given

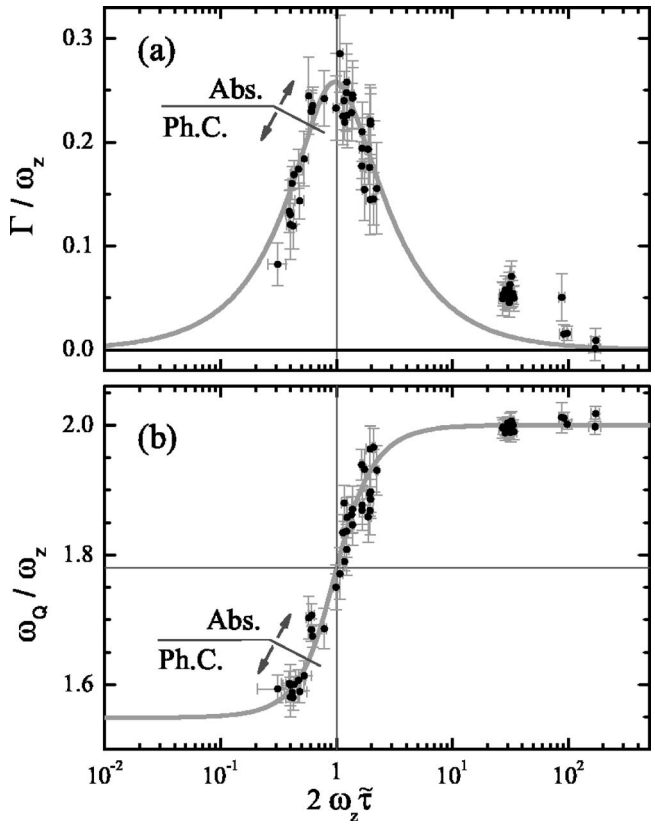

FIG. 5. Damping (raw data) (a) and frequency (extrapolated to harmonic limit) (b) of the quadrupole mode versus scaled relaxation time. The solid line in (a) corresponds to the imaginary part ($\Gamma=-\omega''$) of the solution of Eq. (4); in (b) to the real part ($\omega_Q=\omega'$). The crosshair marks the location of the crossover point. The vertical error bars are identical to Fig. 4, the horizontal ones represent the standard deviations.

in Fig. 5(a) for Γ/ω_z and Fig. 5(b) for ω_Q/ω_z.

From the damping results [Fig. 5(a)] we obtain $2\omega_z\tilde{\tau}_0=1.0(1)$ for the experimental value of the crossover point. Given the 30% absolute accuracy of our density determination this agreement is fortuitously good (see Sec. II).

The determination of the crossover point from the frequency crossover behavior is less straightforward, because errors in the temperature determination add to the error in the extrapolated frequency ω_Q. Further, as the frequency corrections are all positive, they affect the determination of $2\omega_z\tilde{\tau}_0$ from Fig. 5(b). For the crossover region ($0.1\lesssim 2\omega_z\tilde{\tau}\lesssim 10$) the average applied frequency correction was $\delta\omega_Q/\omega_z=2.6\%$, which changes the experimental value for $2\omega_z\tilde{\tau}_0$ by a factor 0.85 to yield $2\omega_z\tilde{\tau}_0=1.0(1)$ [55]. This value coincides with the result obtained from the damping data and shows that our results are self-consistent.

In the collisionless regime anharmonicities can give rise to dephasing induced damping. These effects were not corrected for as they do not affect to leading order the determination of the crossover point. Here we briefly comment on these effects. Roughly, one may argue that for a given anharmonic spread $\delta\omega_Q$ in frequencies the dephasing time δt will be given by $\delta\omega_Q\delta t\approx 2\pi$. Hence, the dephasing related damping rate is $\delta\Gamma=2\pi/\delta t\approx\delta\omega_Q$. The cluster of data points at $2\omega_z\tilde{\tau}\approx 30$ in Fig. 5(a) best illustrates the significance of the correction as they were taken at the highest temperature (9 μK). For these points the anharmonic frequency shift $\delta\omega_Q$ is $\sim$3.5% (see Fig. 3). With $\delta\Gamma/\omega_z\simeq\delta\omega_Q/\omega_z=0.035$ this suggests that the anomalously high damping rates observed for these data points [Fig. 5(a)] may be entirely attributed to dephasing effects. Near the crossover point the collisional damping is much faster and dephasing corrections may be neglected $\delta\Gamma/\Gamma\simeq(1/2)(\delta\omega_Q/\Gamma)^2\approx 10^{-3}$.

We also verified that our shot-to-shot variations in the density have a negligible effect on the measured damping rate. The frequency shifts fastest at the density of the crossover point, where $\delta(\omega_Q/\omega_z)/\delta(\omega_{\rm cl}\tilde{\tau})=(2/\pi)(\omega_{\rm cl}-\omega_{\rm hd})/\omega_z\approx 0.3$ as follows directly by taking the first derivative of Eq. (6) with respect to $\tilde{\tau}$. As $\tilde{\tau}$ scales inversely proportional to the central density, a 1% variation in atom numbers results (at constant temperature) in a $\sim$0.3% variation of the frequency, which is much smaller than the one considered above and therefore also negligible.

VI. SUMMARY AND CONCLUSIONS

With Figs. 4 and 5 we obtain good agreement between experiment and the crossover theory. The frequency shifts down from $2\omega_z$ in the collisionless regime to $1.55\omega_z$ for collisionally hydrodynamic clouds, with ω_z the axial frequency of our trap. Most of the shift occurs over a narrow range of densities around the crossover point. The damping rate peaks over the same range of densities. The determinations of the crossover point from the frequency and the damping behavior agree within 10%, $2\omega_z\tilde{\tau}_0=1.0(1)$. The agreement with the theory is limited by a 30% absolute uncertainty in density. Further, we present a theory and experimental evidence for anharmonic frequency shifts. The theory allows numerical evaluation for potentials with known first and second spatial derivatives. We show that for elongated Ioffe-Pritchard traps knowledge of the central field B_0 suffices to calculate the leading anharmonic shifts with simple analytic expressions.

ACKNOWLEDGMENTS

The authors wish to thank Steve Gensemer, Mikhail Baranov, and Jérémie Léonard (JL) for valuable discussions and JL also for providing data from his thesis. JTMW benefited from participation in the program on quantum gases of the Kavli Institute for Theoretical Physics (KITP) in Santa Barbara. This work is part of the research program on cold atoms of the Stichting voor Fundamenteel Onderzoek der Materie (FOM), which is financially supported by the Nederlandse Organisatie voor Wetenschappelijk Onderzoek (NWO).

[1] L. P. Pitaevskii and S. Stringari, *Bose-Einstein Condensation* (Clarendon Press, Oxford, 2003).
[2] E. M. Lifschitz, and L. P. Pitaevskii, *Physical Kinetics* (Butterworth-Heinemann, Oxford, 1981).
[3] L. D. Landau, and E. M. Lifschitz, *Fluid Mechanics* (Butterworth-Heinemann, Oxford, 1987).
[4] M. Knudsen, Ann. Phys. **28**, 75 (1908).
[5] Yu. Kagan, E. L. Surkov, and G. V. Shlyapnikov, Phys. Rev. A **55**, R18 (1997).
[6] A. Griffin, Wen-Chin Wu, and S. Stringari, Phys. Rev. Lett. **78**, 1838 (1997).
[7] T. Nikuni and A. Griffin, J. Low Temp. Phys. **111**, 793 (1998).
[8] K. M. O'Hara, S. L. Hemmer, M. E. Gehm, S. R. Granade, and J. E. Thomas, Science **298**, 2179 (2002).
[9] C. A. Regal and D. S. Jin, Phys. Rev. Lett. **90**, 230404 (2003).
[10] T. Bourdel, J. Cubizolles, L. Khaykovich, K. M. F. Magalhães, S. J. J. M. F. Kokkelmans, G. V. Shlyapnikov, and C. Salomon, Phys. Rev. Lett. **91**, 020402 (2003).
[11] S. Stringari, Europhys. Lett. **65**, 749 (2004).
[12] D. M. Stamper-Kurn, H. J. Miesner, S. Inouye, M. R. Andrews, and W. Ketterle, Phys. Rev. Lett. **81**, 500 (1998).
[13] M. Leduc, J. Léonard, F. Pereira dos Santos, E. Jahier, S. Schwartz, and C. Cohen-Tannoudji, Acta Phys. Pol. B **33**, 2213 (2002).
[14] S. D. Gensemer and D. S. Jin, Phys. Rev. Lett. **87**, 173201 (2001).
[15] F. Toschi, P. Capuzzi, S. Succi, P. Vignolo, and M. P. Tosi, J. Phys. B **37**, No. 7, S91–S99 (2004); F. Toschi, P. Vignolo, S. Succi, and M. P. Tosi, Phys. Rev. A **67**, 041605(R) (2003).
[16] I. Shvarchuck, Ch. Buggle, D. S. Petrov, K. Dieckmann, M. Zielonkovski, M. Kemmann, T. Tiecke, W. von Klitzing, G. V. Shlyapnikov, and J. T. M. Walraven, Phys. Rev. Lett. **89**, 270404 (2002).
[17] Ch. Buggle, I. Schvarchuck, W. von Klitzing, and J. T. M. Walraven, J. Phys. IV **116**, 211 (2004).
[18] I. Shvarchuck, Ch. Buggle, D. S. Petrov, M. Kemmann, W. von Klitzing, G. V. Shlyapnikov, and J. T. M. Walraven, Phys. Rev. A **68**, 063603 (2003).
[19] F. Gerbier, J. H. Thywissen, S. Richard, M. Hugbart, P. Bouyer, and A. Aspect, Phys. Rev. Lett. **92**, 030405 (2004).
[20] M. Greiner, C. A. Regal, and D. S. Jin, Nature (London) **426**, 537 (2003).
[21] S. Jochim, M. Bartenstein, A. Altmeyer, G. Hendl, S. Riedl, C. Chin, J. Hecker Denschlag, and R. Grimm, Science **302**, 2101 (2003).
[22] J. Cubizolles, T. Bourdel, S. J. J. M. F. Kokkelmans, G. V. Shlyapnikov, and C. Salomon, Phys. Rev. Lett. **91**, 240401 (2003).
[23] M. W. Zwierlein, C. A. Stan, C. H. Schunck, S. M. F. Raupach, S. Gupta, Z. Hadzibabic, and W. Ketterle, Phys. Rev. Lett. **91**, 250401 (2003).
[24] T. Nikuni and A. Griffin, Phys. Rev. A **69**, 023604 (2004).
[25] S. Chapman and T. G. Cowling, *The Mathematical Theory of Non-Uniform Gases* (Cambridge University Press, Cambridge, 1970).
[26] Because the flow is irrotational shear viscosity plays no role and viscous damping is absent. Because the flow is divergence-free the temperature is constant.
[27] G. M. Kavoulakis, C. J. Pethick, and H. Smith, Phys. Rev. A **57**, 2938 (1998).
[28] D. Guéry-Odelin, F. Zambelli, J. Dalibard, and S. Stringari, Phys. Rev. A **60**, 4851 (1999).
[29] U. Al Khawaja, C. J. Pethick, and H. Smith, J. Low Temp. Phys. **118**, 127 (2000).
[30] P. Pedri, D. Guéry-Odelin, and S. Stringari, Phys. Rev. A **68**, 043608 (2003).
[31] K. Dieckmann, R. J. C. Spreeuw, M. Weidemüller, and J. T. M. Walraven, Phys. Rev. A **58**, 3891 (1998).
[32] T. G. Tiecke, M. Kemmann, Ch. Buggle, I. Schvarchuck, W. von Klitzing, and J. T. M. Walraven, J. Opt. B: Quantum Semiclassical Opt. **5**, S119–S123 (2003).
[33] The depletion is done with our detection laser. For absorption imaging we typically use 5% of the full detection intensity (2.4 mW) for typically 10 ms at a detuning of 32 MHz red to the $(5S_{1/2},F=2)\leftrightarrow(5P_{3/2},F=3)$ transition (D_2 line). For phase-contrast imaging we use $>80\%$ of the full detection intensity at a detuning of -3 GHz for a duration of up to 100 ms.
[34] For a full derivation, see Ch. Buggle, Ph.D. thesis, University of Amsterdam.
[35] T. Bergeman, G. Erez, and H. J. Metcalf, Phys. Rev. A **35**, 1535 (1987).
[36] E. L. Surkov, J. T. M. Walraven, and G. V. Shlyapnikov, Phys. Rev. A **49**, 4778 (1994).
[37] The gravitational force mg is small as compared to the gradient of the radial trapping field, $mg/\mu_B\alpha\approx 0.04$. Therefore gravity corrections may be neglected to lowest order in the expansion.
[38] The lasers for phase-contrast and absorption imaging in our experiment are separate devices, the first operating in a region of ± 3 GHz (no online control), the second from -32 to $+15$ MHz (online control) with respect to the D_2 line. It was not possible to use both detection methods during the same experimental run.
[39] Type TE/CCD-512 EFT by Princeton Instruments.
[40] We found that phase contrast imaging in the region from -2.8 GHz up to resonance is destructive with frequency dependent levels of particle losses per imaging flash. We attribute this to bound states in the molecular interaction asymptotes of the $(5S_{1/2}-5P_{3/2})$ transition [41] and assume that atoms are photoassociated during detection. These lines are hard to avoid in view the linewidth of our phase contrast imaging laser (~ 2 MHz FWHM) and the density of lines close to the dissociation limit. Using blue detuning we observe a similar loss mechanism. We attribute this to the continuum states of the repulsive branch of the molecular interaction potentials.
[41] M. Kemmann, I. Mistrik, S. Nussmann, H. Helm, C. J. Williams, and P. S. Julienne, Phys. Rev. A **69**, 022715 (2004).
[42] Detection is done with a 40 μs flash of linearly polarized light and for absorption imaging detunings chosen to keep the peak optical density at ~ 2. The polarization and propagation vectors are both orthogonal to the trap axis. The intensity is 2 mW/cm^2. The effects of saturation and optical pumping arise only at small detunings and are corrected for to first order where necessary.
[43] Our optical resolution is 3.3 μm $1/e$ half-width (measured with a positive 1951 USAF resolution target), which is a factor of $\gtrsim 3$ times smaller than the radial $1/e$ half-width of our clouds in the trap. We also calculate, for the detuning and the highest density used for absorption imaging, the maximum angle of the propagation direction of the light wave phase front

from the forward vector after passing the cloud. We find an angle of 6.8°, whereas the numerical aperture of our imaging system (NA=0.15) corresponds to a maximum collection angle of 8.6°. In view of the quality of the imaging achromats, we therefore assume, that "lensing" is absent in all regimes [44].

[44] C. C. Bradley, C. A. Sackett, and R. G. Hulet, Phys. Rev. A **55**, 3951 (1997).

[45] W. Ketterle, D. S. Durfee, and D. M. Stamper-Kurn, in *Making, Probing, and understanding Bose-Einstein Condensates*, Proceedings of the International School of Physics, "Enrico Fermi," Course CXL, edited by M. Inguscio, S. Stringari, and C. E. Wieman (IOS Press, Amsterdam, 1999), pp. 67–359.

[46] K. Dieckmann, Ph.D. thesis, University of Amsterdam.

[47] E. G. M. van Kempen, S. J. J. M. F. Kokkelmans, D. J. Heinzen, and B. J. Verhaar, Phys. Rev. Lett. **88**, 093201 (2002).

[48] This accuracy is limited by our knowledge of the effective absorption cross section for the $(5S_{1/2},F=2)\leftrightarrow(5P_{3/2},F=3)$ transition. We measured a linewidth 30% larger than the literature value (see H. J. Metcalf and P. van der Straten, *Laser Cooling and Trapping* (Springer Verlag, New York, 1999).

[49] We note that L_e is obtained from the column density and does not coincide with the effective length of the cloud. In contrast to harmonic traps, in anharmonic traps the value obtained for the Gaussian length of a thermal cloud by fitting a 2D Gaussian to the column density differs in general from the value obtained by fitting a 3D Gaussian to the full density distribution of the same cloud.

[50] D. Guéry-Odelin, Phys. Rev. A **66**, 033613 (2002).

[51] J. Léonard, Ph.D. thesis, ENS-Paris. Note, that in the experiment described therein a different element (*He), a different trap (QUIC-trap), and different values for B_0 were used.

[52] Further investigation of this anharmonicity or reacquisition of the quadrupole oscillation data was not possible, since the experimental apparatus was disassembled prior to the completion of data analysis.

[53] J. Söding, D. Guéry-Odelin, P. Desbiolles, F. Chevy, H. Inamori, and J. Dalibard, Appl. Phys. B: Lasers Opt. **69**, 257 (1999).

[54] In the collisionless limit frequency shifts as small as 1% are significant (see Fig. 4). For our trap anharmonic shifts of that size are expected for $T\gtrsim 2\ \mu$K.

[55] The quoted error corresponds to a conservative (factor of 2) uncertainty in the slope of the correction curve.